Electronic structure of nickelates: From two-dimensional heterostructures to three-dimensional bulk materials

P. Hansmann,[1] A. Toschi,[1] Xiaoping Yang,[2] O. K. Andersen,[2] and K. Held[1]

[1]*Institute for Solid State Physics, Vienna University of Technology, 1040 Vienna, Austria*
[2]*Max-Planck-Institut für Festkörperforschung, 70569 Stuttgart, Germany*

Reduced dimensionality and strong electronic correlations, which are among the most important ingredients for cupratelike high-T_c superconductivity, characterize also the physics of nickelate-based heterostructures. Starting from the local-density approximation we arrive at a simple two-band model for quasi-two-dimensional (2D) $LaNiO_3/LaAlO_3$ heterostructures and extend it by introducing an appropriate hopping in the z direction to describe the dimensional crossover to three dimensions (3D). Using dynamical mean-field theory, we study the effects of electronic correlations with increasing interaction strength along the crossover from 2D to 3D. Qualitatively, the effects of electronic correlations are surprisingly similar, albeit quantitatively larger interaction strengths are required in three dimensions for getting a Mott-Hubbard insulating state. The exchange parameters of an effective Kugel-Khomskii-type spin-orbital model are also derived and reveal strong antiferromagnetic tendencies.

I. INTRODUCTION

With the tremendous experimental progress[1] in growing oxide heterostructures, new routes to engineer the dimensionality of materials have become available. A physical phenomenon particularly sensible to dimensionality is high-T_c superconductivity[2] which seems to find its ideal playground in quasi-two-dimensional (2D) systems. Maybe not accidentally, in two dimensions also strong antiferromagnetic spin fluctuations prosper, without undergoing a phase transition to long-range order as in three dimensions.

Besides two dimensionality, the electronic structure of the most prominent class of unconventional superconductors, the cuprate family, is governed by a single Cu $d_{x^2-y^2}$ orbital doped slightly away from half filling. An important step toward a better understanding of cuprate superconductivity was taken by Pavarini *et al.*[3] who found an empirical trend in the material dependence of the critical temperature, T_c, at optimal doping. In the proposed scenario the material dependent parameter is the energy difference between the *planar* Cu $d_{x^2-y^2}$ orbital at the Fermi energy and an *axial* Cu 4*s*-like orbital at higher energy.

In a recent letter,[4] Chaloupka and Khaliullin proposed the artificial engineering of nickelate heterostructures with the aim of getting cupratelike electronic structure and interplay between axial and planar orbitals. A possible realization are $LaNiO_3$=LaO-NiO₂ layers alternated with insulating layers such as $LaAlO_3$=LaO-AlO₂ with the same sequence of sublayer charges. To avoid macroscopic polarization, the substrate on which the heterostructure is grown should preferably have the same sequence of sublayer charges ($SrTiO_3$ may for instance not be suitable). We have shown that in these d^7 heterostructures, the Ni $d_{3z^2-r^2}$ orbital can play the role of the *axial* orbital;[5] it is pushed considerably above the planar Ni $d_{x^2-y^2}$ orbital as an effect of either the Coulomb interaction, an axially compressive strain, or control of the apical cation (substitution of Al by, e.g., Sc) (Ref. 6) so that a single-Fermi-surface sheet with similar geometry and vol-

ume as in cuprates emerges, before the system becomes eventually insulating. These theoretical studies triggered a considerable experimental effort to find superconductivity in Nickel based heterostructures.[7–9]

The main focus of this complementary paper is a detailed analysis of the Mott-Hubbard transition taking place in the *axial*/*planar* two-band system and of the changes observed when going from the two-dimensional heterostructure to three-dimensional (3D) bulk nickelates. The latter can be viewed as a dimensional crossover, in which the Cu $d_{3z^2-r^2}$ degrees of freedom are more equivalent to the Cu $d_{x^2-y^2}$ ones due to the lack of dimensional constraint.

For the purpose of this study, we simplify the local-density-approximation (LDA) band structure of Ni e_g orbitals by including merely the hopping between the first- and second-nearest neighbor Ni $d(e_g)$ Wannier orbitals, in contrast to Ref. 5 where the full LDA band structure was considered. This gives a quarter-filled two-band model for the e_g degrees of freedom, i.e., one electron in the two Ni e_g orbitals. We recall here that in transition-metal oxides the transition-metal ion is usually surrounded by an oxygen octahedron and, depending on the specific case, either t_{2g} (as, e.g., in vanadium sesquioxide) states or e_g states (as in the nickelates and cuprates) play the most important role in determining the low energy excitations of the system. Hence, our study of an e_g-band model at quarter filling and the dimensional crossover from quasi-two-dimensional to quasi-three-dimensional systems is of interest also from a more general perspective. Moreover, since there are plenty of parameters governing the physics such as the bandwidth of the two bands, their crystal-field splitting, the interband hybridization, the Coulomb interaction, and last but not least the dimensionality, it is of great importance to derive such models from realistic band structures.

This way we also make some contact to previous multiband model studies,[10–17] where features such as the orbital selective Mott transitions[18–20] were analyzed. Many of these multiband studies made approximations, such as neglecting

the hybridization between the orbitals. This poses the question in how far the employed models are applicable to real world materials. Moreover, most of the aforementioned studies concentrated on half filling.

In Sec. II, we will briefly discuss the two-band model and how we derive its parameters. In Sec. II B, we discuss the evolution of the spectral function, self-energy and double occupation with increasing Coulomb interaction strength. In Sec. III, we turn to the dimensional crossover, comparing the quasi-two-dimensional system for a heterostructure and a more homogeneous 3D model. Finally, we discuss the issue of magnetic order at low temperatures and derive an effective spin-orbital superexchange model in Sec. IV, before we arrive at the conclusion in Sec. V.

II. LDA+DMFT

A. Effective two-band model

Density-functional calculations were performed for the simplest, 1/1 unstrained superlattice $LaNiO_3/LaAlO_3$ $=LaO$-NiO_2-LaO-AlO_2 of which a detailed discussion can be found in Ref. 5. Here we recall the most important facts relevant for the discussion of our model study. In the $LaNiO_3/LaAlO_3$ heterostructure nickel is in a trivalent state Ni^{3+}. The coordination polyhedron is an octahedron with a small tetragonal distortion due to the $LaAlO_3$ layers along the c axis. The cubic crystal-field eigenstates of the Nickel d electrons are the lower lying t_{2g} triplet and the higher lying e_g doublet. The cubic splitting is large enough so that the nominal filling in Ni^{3+} is t_{2g}^6 (completely filled) and e_g^1 (quarter filling). As a consequence we find two e_g bands at quarter filling around the Fermi energy to be the relevant degrees of freedom for the low energy excitations of the system.[5] The insulating $LaAlO_3$ layers give rise to the tetragonal distortion which splits the axial $|3z^2-r^2\rangle$ orbital ≈ 150 meV above the $|x^2-y^2\rangle$ orbital and, more importantly, strongly reduce the width of the axial $|3z^2-r^2\rangle$ band by blocking the perpendicular hopping.[5]

In order to obtain the model for our dynamical mean field (DMFT) study we construct a basis of localized Ni e_g Wannier functions using the Nth-order muffin-tin orbital method (NMTO) like in Ref. 5 but now truncate the hoppings after those between second-nearest Ni neighbors. For our purposes of model calculations we prefer this simpler picture of the systems kinetics in real space and pay the price of a slightly less accurate representation of the dispersion of the LDA conduction bands. Let us remark that this simplification could affect the Fermi-surface transition discussed in Ref. 5 but not the overall properties of the metal-insulator transition (MIT) and the 2D to 3D crossover.

In the basis $\{|x^2-y^2\rangle, |3z^2-r^2\rangle\}$ of the planar and axial e_g Bloch-summed orbitals, the one-electron part of the Hamiltonian is

$$\varepsilon_{\mathbf{k}}^{2D} = -2(\cos k_x + \cos k_y)\begin{pmatrix} 0.45 & 0 \\ 0 & 0.17 \end{pmatrix} + 2(\cos k_x - \cos k_y)$$

$$\times \begin{pmatrix} 0 & 0.28 \\ 0.28 & 0 \end{pmatrix} - 4(\cos k_x \cos k_y)\begin{pmatrix} 0.09 & 0 \\ 0 & 0.03 \end{pmatrix}$$

$$+ \begin{pmatrix} 0 & 0 \\ 0 & 0.15 \end{pmatrix}. \tag{1}$$
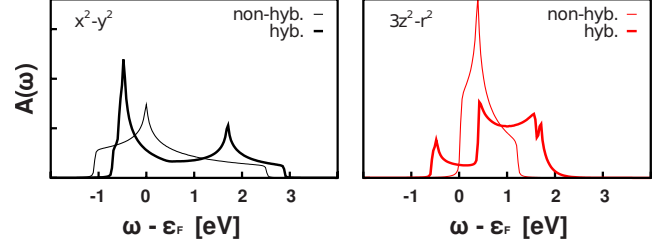

FIG. 1. (Color online) Orbitally projected DOS (spectral density) for each of the two e_g bands (thick lines). Neglecting the interorbital hybridization leads to the results shown as thin lines. The hybridization is seen to strongly enhance the width of the $3z^2-r^2$ spectral density, leading to a remarkable itinerancy, despite the quasi-two-dimensional nature of the $LaNiO_3/LaAlO_3$ heterostructure.

Here, energies are in electron volts. The first and second terms account for, respectively, the intraorbital and interorbital nearest-neighbor hoppings. We see that the hopping between the x^2-y^2 orbitals is almost three times as large as the one between the $3z^2-r^2$ orbitals and that the interorbital hopping is nearly the geometrical average of the intraorbital hoppings. This, as well as the factor of 3, is what one expects when the Ni-Ni hopping is exclusively via O, i.e., when $t_{Ni-Ni}=t_{Ni-O}t_{O-Ni}/(\varepsilon_{Ni}-\varepsilon_O)$ and t_{Ni-O} follows the canonical rules,[31] which in the present case yield: $t_{x^2-y^2}=\sqrt{3}t_{3z^2-r^2}$ in x and y directions. The third term in Eq. (1) is the second-nearest-neighbor hopping and the fourth is the on-site term, i.e., it gives the tetragonal crystal-field splitting. The two last-mentioned terms do not mix the two orbitals. In real space, the Hamiltonian of our effective model reads

$$\hat{H}_{mod.} = \sum_{iljm,\sigma} t_{iljm}c_{il\sigma}^\dagger c_{jm\sigma} + \hat{H}_{int.}, \tag{2}$$

where $l,m \in \{p,a\}$ label the planar and axial orbitals. The hopping amplitudes t_{iljm} are the matrices in Eq. (1) with l,m as the orbital index and i,j as site index of nearest or next-nearest neighbors on the square lattice.

The effects of the interorbital hybridization are clearly visible in Fig. 1 showing the noninteracting density of states (DOS) resulting from the noninteracting first part of Hamiltonian (2). A comparison to the case without hybridization ($t_{pa}=0$) plotted as a thin line shows a big difference especially for the $3z^2-r^2$ projection. Its width is strongly enhanced if the hopping to the more mobile x^2-y^2 orbitals is properly taken into account. This effect is important since otherwise the reduced hopping in the z direction would more severely reduce the itinerancy of electrons in the $3z^2-r^2$ orbital.[21] That is, in the absence of the x^2-y^2 to $3z^2-r^2$ hybridization the $3z^2-r^2$ orbitals would localize too easily (even at a small Coulomb interaction strength). This scenario was originally proposed in Ref. 4 prior to realistic material calculations.

The Coulomb interaction terms read

$$\hat{H}_{int.} = U\sum_{il\sigma} n_{il}^\uparrow n_{il}^\downarrow + \sum_{il>m\sigma\sigma'} (V-\delta_{\sigma,\sigma'}J)n_{il}^\sigma n_{im}^{\sigma'}, \tag{3}$$

where $n_{il}^\sigma = c_{il\sigma}^\dagger c_{il\sigma}$, $\delta_{\sigma,\sigma'}$ denotes the Kronecker symbol, U and V represent the intraorbital and interorbital repulsion,

respectively, and J is the Hund exchange term.

For the solution of the impurity problem in the DMFT self-consistency loop we use quantum Monte Carlo simulations of the Hirsch and Fye-type,[22] where neither the pair hopping term (corresponding to highly excited states) nor the spin-flip term (which poses a severe sign problem in the numerical simulation[23]) have been included. Presented results were obtained at $\beta=10$ eV^{-1} except for the double occupancies shown in the right panel of Fig. 5. Further, convergence with respect to the value of the Trotter discretization $\Delta\tau$ was validated. Afterward, the maximum entropy method was employed to perform analytic continuation of the Green's function to the real axis. Concerning the choice of the interaction parameter we perform a systematic analysis, where U is varied in a regime of physically meaningful values in order to investigate the Mott transition and its specific features. The Hund's exchange term, on the other hand, has been fixed to $J=0.7$ eV, a reasonable value close to that of atomic Ni. Moreover, assuming the deviation from cubic symmetry to be negligible with respect to the Coulomb interaction parameters, we employ $V=U-2J$.

Before presenting our numerical results a comment about the applicability of DMFT to the finite-dimensional system considered is due. While it has been shown that corrections arising from spatial correlations beyond DMFT (Refs. 24 and 25) are generally small in 3D (except in the close proximity of a second-order phase transition), stronger effects have to be expected for 2D systems. The strength of such correction with respect to DMFT is, however, decreasing with increasing temperatures[25,26] and therefore can be neglected as a first approximation in the temperature regime we are considering here. This corresponds to the assumption that we are well above any ordering temperature at $\beta=10-25$ eV^{-1}. Naturally a different treatment to include effects of spatial correlations is necessary in order to study the low-temperature regime where spin fluctuations and, possibly, superconductivity emerge. For this reason we include in Sec. IV a two-site calculation to estimate the size of nonlocal antiferromagnetic correlations for the system considered.

B. Mott transition in two dimensions

1. Spectral function and self-energy

Figure 2 shows the evolution of the k-integrated spectral functions $A(\omega)$ for both orbitals with increasing U. Let us first focus on the x^2-y^2-projected spectral density (black curve). Already at $U=4.4$ eV ($V=3.0$ eV; first panel), the spectrum is strongly renormalized with respect to the noninteracting case: a narrow quasiparticle peak at ε_F and Hubbard bands which are separated by an energy of the order of U are well visible. As the value of the interaction parameter is increased to $U=5.4$ eV and $U=6.4$ eV (second and third panels), such spectral features become even more pronounced as one observes a stronger renormalization of the quasiparticle peak and more pronounced Hubbard bands. However, at $U=7.4$ eV (fourth panel) a qualitative change has occurred: the spectral weight at the Fermi level has vanished and a Mott-Hubbard gap has been formed. Hence, a
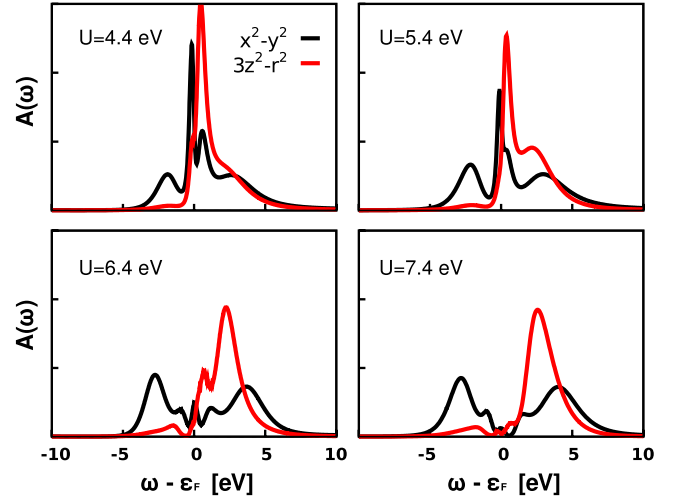

FIG. 2. (Color online) Evolution of the LDA+DMFT spectrum with increasing Coulomb interaction U (with $J=0.7$ eV, $V=U-2J$) at $\beta=10$ eV^{-1}. The black curves show the x^2-y^2 and the red/gray ones the $3z^2-r^2$-projected spectral density.

Mott metal-insulator transition has taken place between $U=6.4$ and 7.4 eV.

Figure 2 also indicates that the metal-insulator transition of the $3z^2-r^2$ band (red/gray curve) occurs for the same critical interaction of $U\gtrsim6.4$ eV as in the x^2-y^2 band. It is, however, qualitatively different. For U increasing from 4.4 eV, one observes that the $3z^2-r^2$ quasiparticle peak is shifted above that of the x^2-y^2 peak, which is at the Fermi level. This is the Coulomb enhancement of the tetragonal crystal field which causes the Fermi surface to have only one, mostly x^2-y^2-like sheet as in the cuprates.[5] For increasing U, the $3z^2-r^2$ spectral weight shifts further and further above the Fermi level where for $U=7.4$ eV it has completely disappeared. The remaining spectral weight below the Fermi energy, corresponding to the lower Hubbard band, is entirely due to the hybridization with the lower x^2-y^2-like Hubbard band.

The different nature of the metal-insulator transition in the x^2-y^2 and the $3z^2-r^2$ bands can be identified even more clearly from an analysis of the self-energy. In Fig. 3, we show the evolution of the imaginary part of the self-energy $\text{Im}\,\Sigma_{x^2-y^2}(\omega_n)$ with increasing interaction. Again, for the x^2-y^2 band, the expected behavior of a standard Mott transition is found. The appearance of the insulating gap results from the divergence of $\text{Im}\,\Sigma_{x^2-y^2}(\omega)$ in the limit of zero frequency. In this limit the quasiparticle renormalization factor $Z=[1-\frac{\partial\,\text{Im}\,\Sigma(i\omega)}{\partial\omega}|_{\omega=0}]^{-1}$ goes to zero as a further hallmark of the Mott character of the transition in the x^2-y^2 band (see black circles in the left panel of Fig. 4). At the same time, however, the insulating transition of the $3z^2-r^2$ band is not associated to any qualitative change in $\text{Im}\,\Sigma_{3z^2-r^2}(\omega)$. For all interactions a "metalliclike" bending can be observed in $\text{Im}\,\Sigma_{3z^2-r^2}(\omega)$ at low frequencies. As a consequence of this, the renormalization factor Z stays always finite (red crosses in the right panel of Fig. 4). The disappearance of spectral weight at the Fermi energy in this case is determined by a large relative shift in the orbitals induced by the Coulomb
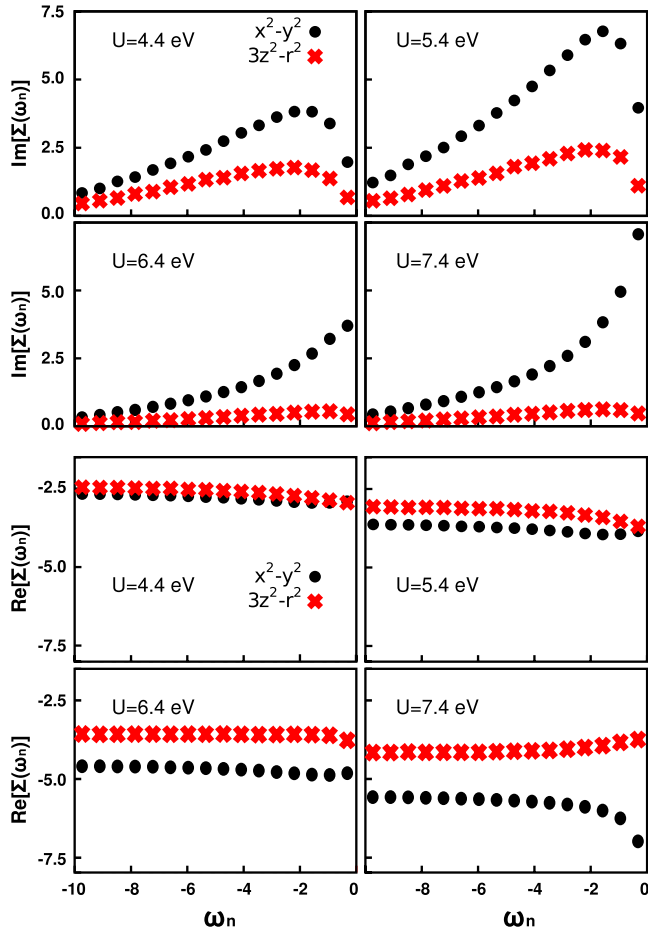
FIG. 3. (Color online) Evolution of the LDA+DMFT self-energy (vs negative Matsubara frequencies) with increasing U at $\beta=10$ eV^{-1}. The black curves show the x^2-y^2 and the red/gray ones the $3z^2-r^2$ self-energy. Via extrapolation of the imaginary and real part of the self-energy to $\omega_n \to 0$ we can obtain the quasiparticle renormalization Z and the "crystal-field" enhancement, respectively, shown in Fig. 4.

FIG. 4. (Color online) Left hand side: effective chemical potential $\mu - \mathrm{Re}\,\Sigma(0)$ relative to the noninteracting chemical potential for the x^2-y^2 (black) and $3z^2-r^2$ (red/gray) orbital at $\beta=10$ eV^{-1}. At the Mott transition, the low frequency effective chemical potential of the $3z^2-r^2$ orbital is strongly reduced so that it is shifted above the Fermi energy, i.e., the $3z^2-r^2$ orbital becomes "band" insulating. Right-hand side: quasiparticle weight Z for the x^2-y^2 (black) and $3z^2-r^2$ (red) orbital (also at $\beta=10$ eV^{-1}). For the x^2-y^2 orbital, we find $Z \to 0$, i.e., the (central) quasiparticle peak disappears and the x^2-y^2 orbital becomes Mott insulating.

interaction. This shift $\Delta_{CF}^{\mathrm{eff}}$, is a consequence of the strong variation in the real part of the self-energies at zero frequency shown in the left panel of Fig. 4. More specifically, while the effective chemical potential of the x^2-y^2 band [defined as $\mu - \mathrm{Re}\,\Sigma_{x^2-y^2}(0)$] remains close to the noninteracting value up to $U=6.4$ eV, its value for the $3z^2-r^2$ band is clearly decreasing with increasing U. As a result, the metal-insulator transition of the $3z^2-r^2$ band occurs for a value of $U \gtrsim 6.4$ eV, when the low-energy spectral weight of this band is shifted above the Fermi energy.

A key feature in the physics we have observed here is the interplay between the two orbitals stemming from the fairly large hybridization in Eq. (1) proportional to $\cos k_x - \cos k_y$. An evident sign of such interplay is the concomitance of the metal-insulator transition in both orbitals. For understanding the underlying physics it is instructive to consider the different possible scenarios for the MIT in a two band system with hybridization.

Increasing the Coulomb interaction has basically two effects (see also Refs. 27 and 28 and, in particular, Ref. 17), double occupancy of a site becomes more expensive and
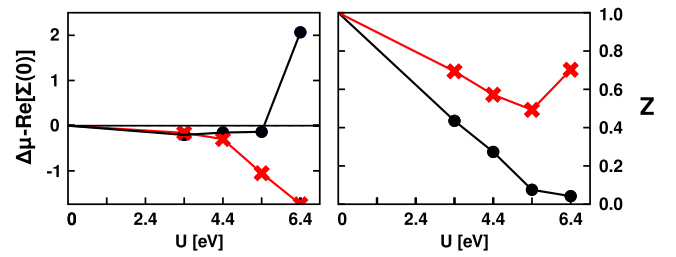
on-site energies of the two orbitals are shifted with respect to each other. This gives rise to three possible transition scenarios. (i) If the shift between the bands is increasing slowly with interaction, double occupancy becomes practically forbidden for a value of V where both bands are still partially filled. As a result, a simultaneous Mott transition occurs with $Z \to 0$ for *both* bands. If, instead, the shift is increasing more rapidly with interaction, at a certain point one of the bands will empty, leaving the other one half filled. The nature of the transition then depends on the value of U for which this happens. There are two possibilities: (ii) if U is strong enough to forbid double occupancy in the half-filled band, this band will become insulating abruptly. Such a situation is reflected in simultaneous, but qualitatively different, metal-insulator transitions for both bands. This is what we observe in Figs. 2 and 3. (iii) The other possibility is that U is not yet strong enough to prevent the double occupancies in the half-filled band. The Mott transition in this band—differently from our case—would then not take place simultaneously with the depletion of the other band. This case is different from the one considered in Figs. 2 and 3 and the only one in which the metal-insulator transition can be fully described in terms of an effective single-band model. The initial lifting of the orbital degeneracy (the LDA crystal-field splitting) is expected to push the system in the direction of situation (ii), which we observed for our model with an initial crystal-field splitting of $\varepsilon_{3z^2-r^2} - \varepsilon_{x^2-y^2} = 150$ meV.

The interorbital hybridization also gives rise to two effects. The first one, which can be understood intuitively, is an effective broadening of the more narrow band (see Fig. 1 for the noninteracting case). This leads to a more metallic behavior of the $3z^2-r^2$ electrons. The second effect is more intrinsic in the sense that the hybridization makes the bands more similar, obviously pushing the system toward situation (i). It is important to notice that both effects work against the effective crystal-field splitting. As mentioned above, the fingerprints of the hybridization can clearly be seen also in Fig. 2. Although the narrow $3z^2-r^2$-like band is shifted above the Fermi energy, at the metal-insulator transition some residual $3z^2-r^2$ weight remains in the region of the lower x^2-y^2-like Hubbard band.
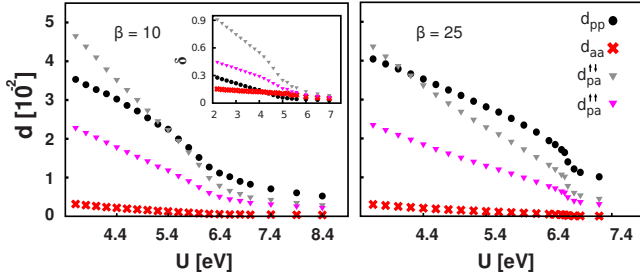
FIG. 5. (Color online) Double occupancy vs Coulomb interaction U for two values of β (left: 10 eV^{-1}; right: 25 eV^{-1}). Shown are the double occupation of the x^2-y^2 orbital (d_{pp}), of the $3z^2-r^2$ orbital (d_{aa}) as well as the double occupation of both orbitals with parallel ($d_{pa}^{\uparrow\uparrow}$) and antiparallel spin ($d_{pa}^{\uparrow\downarrow}$). Inset: double occupancies normalized by the respective density (δ_{mn} see text).

2. Double occupancy

As in the case of the half-filled Hubbard model, complementary information about the metal-insulator transition can be extracted from analysis of the double occupancy d, which is the derivative of the free-energy with respect to the interaction parameter U and is a good indicator for the Mott metal-insulator transition.[29] However, such an analysis for a two-band model is more complicated since it involves not only the orbital-diagonal double occupations ($d_{mm}=\langle n_{m\uparrow}n_{m\downarrow}\rangle$) but also the orbital-offdiagonal parts with parallel ($d_{pa}^{\uparrow\uparrow}=\langle n_{p\uparrow}n_{a\uparrow}\rangle$) and antiparallel spin orientations ($d_{pa}^{\uparrow\downarrow}=\langle n_{p\uparrow}n_{a\downarrow}\rangle$).

The evolution of these four quantities is shown in Fig. 5 for two different temperatures. In both cases we observe the same trend for all double occupations which are decreasing with increasing interaction. Starting the analysis with the x^2-y^2 orbital, which undergoes a Mott-Hubbard transition when getting half filled, we observe that its double occupation decreases around $U=6.4$ eV, i.e., near the critical value of the interaction that we can estimate form the spectral function in Fig. 2. At $kT=1/10$ eV (Fig. 5 left panel), however, this behavior is thermally smeared out. The Mott-Hubbard transition occurs in form of a very smooth crossover. A better estimate can be made by going down in temperature to $kT=1/25$ eV (Fig. 5 right panel), where we can see a very steep drop of d_{pp} marking the transition point at $U\approx7.0$ eV where we also found $Z\to0$ for the x^2-y^2 band.

At a first glance the behavior of the other three double occupancies d_{aa}, $d_{pa}^{\uparrow\downarrow}$, and $d_{pa}^{\uparrow\uparrow}$ appear to be more difficult to interpret. One could have expected that $d_{pa}^{\uparrow\uparrow}$ and $d_{pa}^{\uparrow\downarrow}$ should be the largest ones because they are energetically less expensive ($V, V-J$) in comparison with the d_{mm} (U). What we observe, however, is a crossing of $d_{pa}^{\uparrow\uparrow}$ with d_{pp} at $U\approx5.4$ eV and $U\approx4.2$ eV for $\beta=10$ eV^{-1} and $\beta=25$ eV^{-1}, respectively. Moreover, $d_{pa}^{\uparrow\downarrow}$ is lower than d_{pp} for all interaction values. This situation can be properly understood considering also the depletion of the $3z^2-r^2$ band. The low values of d_{aa}, $d_{pa}^{\uparrow\downarrow}$, and $d_{pa}^{\uparrow\uparrow}$ reflect the low $3z^2-r^2$ electron density. In order to disentangle these effects we have plotted the double occupancies normalized by the respective density in the inset of the left panel of Fig. 5 [$\delta_{mm}=d_{mm}/\langle n_m\rangle^2$, $\delta_{pa}^{\uparrow\downarrow}=d_{pa}^{\uparrow\downarrow}/(\langle n_{p\uparrow}\rangle\langle n_{a\downarrow}\rangle)$, and $\delta_{pa}^{\uparrow\uparrow}=d_{pa}^{\uparrow\uparrow}/(\langle n_{p\uparrow}\rangle\langle n_{a\uparrow}\rangle)$]. In this way the
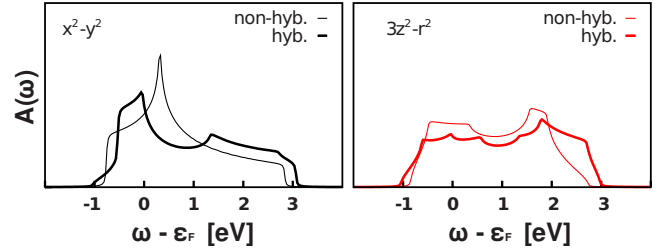

FIG. 6. (Color online) Same noninteracting projected DOS as in Fig. 1 but for the 3D case. The $3z^2-r^2$ band is considerably broader than in the layered 2D case due to the additional hopping in the z direction.

hierarchy of the energetic consideration is restored and all renormalized double occupancies behave in a similar way. On the other hand, the crossing observed in the unrenormalized data can be also interpreted as a clear signal that we are far from the situation (i) described above, that is, a simultaneous Mott-Hubbard transition in both bands.

III. FROM 2D TO 3D

Having discussed in detail the results for the two-dimensional model for the LaAlO$_3$/LaNiO$_3$ superlattice, we now present results for a 3D model for bulk LaNiO$_3$, and compare with the 2D case. Specifically, we no longer restrict the hopping of the axial $3z^2-r^2$ orbital to the xy plane, but allow for hopping along the z axis by adding the term

$$-2t_z\cos(k_z)\begin{pmatrix} 0 & 0 \\ 0 & 1 \end{pmatrix}$$

to the kinetic part of our Hamiltonian (1). We choose $t_z=0.6$ eV, i.e., 4/3 times the 0.45 eV in Eq. (1), as it should be in cubic symmetry according to the Slater-Koster tables[30] and Ref. 31. Our 3D model is not completely cubic because from Eq. (1) we kept the tetragonal crystal-field splitting [last term in Eq. (1)] as well as the second-nearest-neighbor hoppings in xy plane, without including them in the xz and yz planes. Moreover, this 3D model is not to be seen as a true LDA+DMFT analysis of pseudocubic LaNiO$_3$, albeit the link to this compound is a motivation for the analysis of the modified model.

The noninteracting density of states for this 3D model is shown in Fig. 6. The main difference from the 2D model in Fig. 1 is obviously, a much broader $3z^2-r^2$ band caused by the additional hopping in the third direction. As a result of this broadening the two different bands are much more similar than in the 2D case. In the truly cubic case the x^2-y^2 and $3z^2-r^2$ spectral densities would have been identical.

In Fig. 7 we show the spectral functions and self-energies of the interacting 3D system. On the left-hand (right-hand) side the data for a metallic (insulating) solution are plotted. They refer to $U=7.4$ eV and $U=9.9$ eV, respectively. This indicates that the metal-insulator transition occurs for considerably larger values of the interaction than in the 2D system, as might be expected. Another difference to the 2D case is the enhanced spectral weight of the $3z^2-r^2$ band below the
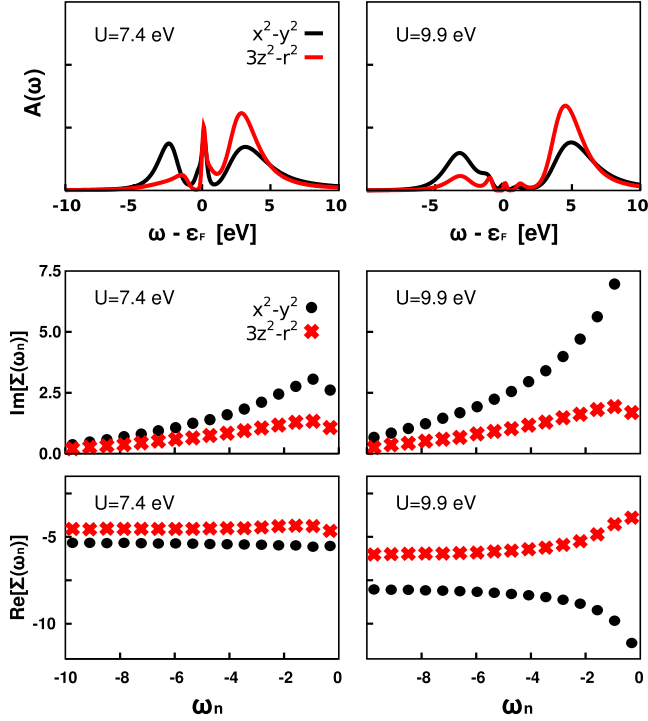
FIG. 7. (Color online) Evolution of the spectrum and the LDA+DMFT self-energy (vs Matsubara frequencies) with increasing Coulomb interaction $V = U - 2J$ for the 3D case at $\beta = 10$ eV^{-1}. The black curves show the $x^2 - y^2$ spectrum and the red/gray ones the $3z^2 - r^2$ spectrum.

Fermi energy. However, the metal-insulator transitions for the two bands are qualitatively similar to those of the 2D case as is clearly demonstrated by the behavior of the imaginary part of the self-energy shown in the bottom panels of Fig. 7. The evolution of the self-energies qualitatively resembles the one shown in Fig. 3 displaying the same "metallic" down bending. The only (quantitative) difference to be noticed with respect to the 2D case is a larger imaginary part of the $3z^2 - r^2$ self-energy at low frequencies. This can be understood as a natural consequence of the closer resemblance of the bands in the noninteracting density of states. In terms of our precedent discussion we thus observe again the situation (ii) of Sec. II B, i.e., a simultaneous albeit quantitatively different Mott transition. However, we are now slightly closer to the case (i) of a simultaneous double Mott transition for both bands than for the layered model. In other words, the Mott transition is qualitatively the same for the 3D as the 2D case but quantitatively the Mott transition is shifted to much higher values of the interaction strength. Such large values can hardly be realized in experiment.

It must however be emphasized that for a truly cubic 3D model, the two e_g orbitals remain identical (for all strengths of the interaction) so that the Mott transition will occur simultaneously for both bands and for a value of U which is about $\sqrt{2}$ larger than for the single-band case.[32] That a small symmetry breaking at the LDA level, as exhibited by our 3D e_g^1 model, can drastically change the nature of the Mott
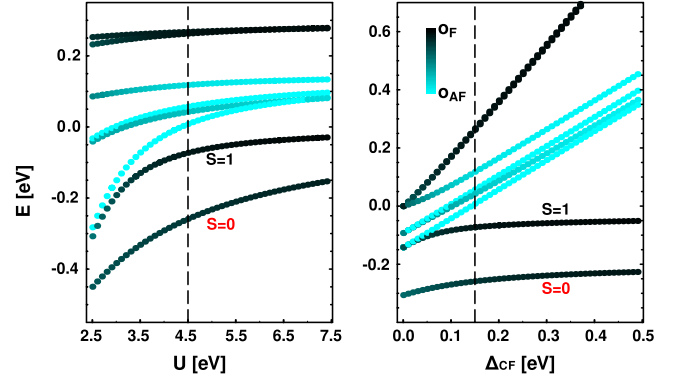

FIG. 8. (Color online) Left hand side: energy level diagram of the two site model as a function of the Coulomb repulsion U for $\Delta_{CF} = 0.15$ eV (dashed line in the plot on the right-hand side). Right hand side (reproduced from Ref. 5): same diagram as a function of Δ_{CF} for $U = 4.5$ eV (dashed line in the plot on the left-hand side). The color of the points indicates the character of orbital ordering (o_F: orbital ferro; o_{AF}: orbital antiferro).

transition in the paramagnetic state has previously been found in DMFT calculations for 3D t_{2g}^2 systems[27,28] and t_{2g}^1 systems,[33] as well as for the e_g^1 system LaMnO$_3$.[34]

IV. PREDOMINATING SPIN FLUCTUATIONS AND EFFECTIVE SUPEREXCHANGE MODEL

A. Predominating spin fluctuations

The model calculations discussed in the previous sections were performed for the paramagnetic phase. However, one expects the system to display magnetic and/or orbital order at sufficiently low temperatures. The treatment of such complex ordered phases is particularly difficult in LDA+DMFT. An insight into this physics can be obtained however by diagonalizing a "two-site version" of Hamiltonian (2) (with open boundary conditions, i.e., a diatomic molecule directed along the x axis). The analysis of the corresponding energy levels for this two-electron system allows to infer the relevant fluctuations which dominate the low-temperature physics. On the left-hand side of Fig. 8 we show the calculated energy-level diagrams as a function of U for the same set of parameters that we have used for the LDA+DMFT 2D crystal calculation discussed in previous sections.

For the values of U considered, the mixing of the lowest energy levels with the energy-costly double-occupied states is very small, i.e., these states are already above the energy window which we plot in Fig. 8. More interestingly, our results show that the ground state of the two site system is always a spin singlet with the two electrons residing predominantly in the same orbital ($x^2 - y^2$) on each site. The splitting of the singlet ground state and the excited triplet is large, and, in the large U limit, it can be regarded as an exchange integral of $J_{ex.} \approx 200$ meV. This indicates an instability of the system at low temperatures toward a spin antiferro-ordered state and orbital ferro-ordered state. We have also studied the effect of varying the initial level (i.e., crystal field) splitting for a reasonable value of $U = 5$ eV (right-hand side of Fig. 8). The main effect of an enhance-
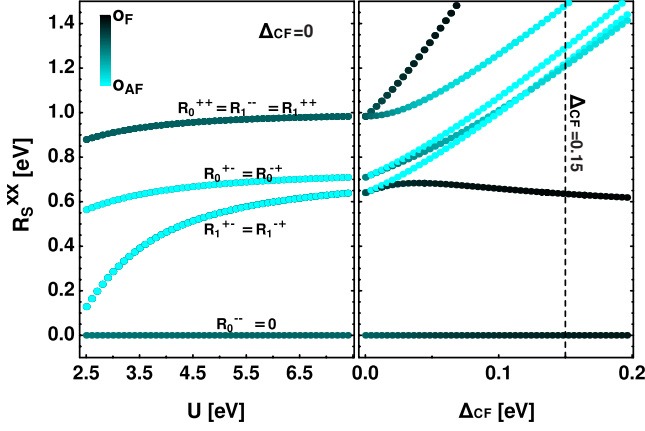
FIG. 9. (Color online) Left hand side: evolution of the R coefficients of Hamiltonian (4) as a function of the interaction parameter U calculated with the two site model in the x^2-y^2 and $3z^2-r^2$ basis for $\Delta_{CF}=0$ eV. Right hand side: evolution with increasing crystal-field splitting starting from the largest U value of the left panel ($U=7.5$ eV). The color of the points indicates the character of orbital ordering with the same scale as in Fig. 8.

ment of the crystal-field splitting is to strengthen the tendency toward ferrotype orbital ordering (of the x^2-y^2 and the $3z^2-r^2$ states) eventually leading to purely one-band physics with only the x^2-y^2 orbital involved.

B. Effective superexchange model

A first analysis of the magnetic and orbital ordered phases in the La_2NiAlO_6 heterostructure was carried out in Ref. 4 considering the following superexchange Hamiltonian, defined for a bond $ij \| \gamma$ in the NiO_2 plane

$$H_{ij}^{(\gamma)} = (R_{\sigma,\pm,\pm} + R_{\sigma,\pm,\pm}^{CT})\left(\frac{1}{2} \pm \hat{\tau}_i^{(\gamma)}\right)\left(\frac{1}{2} \pm \hat{\tau}_j^{(\gamma)}\right)\hat{P}_{\sigma,ij} \quad (4)$$

with an implied sum over $\sigma=0,1$ and all combinations of $\pm,\pm$. $\hat{P}_{\sigma,ij}$ represents the projector to a singlet and a triplet state of two Ni^{3+} $S=\frac{1}{2}$ spins while $\frac{1}{2} \pm \hat{\tau}_j^{(\gamma)}$ selects the planar orbital in the plane perpendicular to the γ axis and the directional orbital along this axis.

Neglecting the charge-transfer part of Hamiltonian (4) allows for a comparison with our two-site calculation, albeit only for $\Delta_{CF}=0$ eV since otherwise Hamiltonian (4) has another orbital symmetry than the full Hamiltonian. In this way we can perform the first numerical estimate of the $R_{\sigma,\pm,\pm}$ coefficients of the superexchange Hamiltonian (4) as a function of the parameter of the microscopic Hamiltonian. More specifically, the $R_{\sigma,\pm,\pm}$ coefficients of Fig. 9 are calculated form the level splitting seen in Fig. 8 which, in turn, depends on the values of the parameters U, J, and t of Hamiltonian (2). The result of this comparison are shown in the left panel of Fig. 9, where for simplicity we assumed the two orbitals to be degenerate.

It is important to note here that the orbital projectors in Eq. (4) do not refer to the x^2-y^2 and $3z^2-r^2$ basis we have

used so far since the γ axis is lying in the NiO_2 plane. This is also reflected in the mixed color of the R_{--}^0 coefficient which corresponds to the singlet ground state.

Finally, in the right panel we show the effect of turning on the crystal-field splitting Δ_{CF}, disregarding some (here still small) terms which admix the orbitals in Hamiltonian (4). The changes in the color clearly indicates a rapid demixing of the eigenstates since the x^2-y^2 and $3z^2-r^2$ orbitals are eigenfunctions of the crystal-field operator. This limits the applicability of Hamiltonian (4) to the cases of small crystal-field splitting.

As for the magnetic fluctuations, the Kugel-Khomskii-type Hamiltonian (4) clearly favors an antiferromagnetic spin alignment along each pair. Depending on the crystal-field splitting, the preferred orbital orientation is along the bond or—for larger crystal field—a ferro-orbital occupation of the x^2-y^2 orbital.

V. CONCLUSION

We have analyzed in detail the Mott transition in the high-temperature, paramagnetic state of $LaAlO_3/LaNiO_3$ heterostructures, including the dimensional crossover from the two-dimensional layered heterostructure to the three-dimensional bulk system. The LDA band structure was NMTO downfolded to the Ni e_g orbitals and, in order to concentrate on the essentials of the Mott physics, we included merely the hoppings between first- and second-nearest Ni neighbors. This realistic model also allowed us to contribute to the intensive discussion on the orbital-selective Mott transition,[10–20] a discussion which with a few exceptions[17] has hitherto neglected the effect of interband hybridization. This hybridization turned out to be most important for the itinerancy of the $3z^2-r^2$ band and for a simultaneous, albeit different Mott transition in both orbitals.

For realistic U values we find that $LaNiO_3/LaAlO_3$ is a metal with an (x^2-y^2)-like quasiparticle peak at the Fermi level and a $(3z^2-y^2)$-like peak slightly above. At larger values of the Coulomb interaction, the $3z^2-r^2$ spectral density is shifted above the Fermi as in a *metal* to *band-insulator* transition for this band while the x^2-y^2-like band undergoes a genuine Mott transition with divergent effective mass ($1/Z$). Due to the hybridization between both orbitals, there is however still spectral weight in the $3z^2-r^2$ channel at the position of the predominately x^2-y^2 lower Hubbard band.

If $LaAlO_3/LaNiO_3$ is grown on a substrate, stress can further enhance the initial (LDA) orbital splitting so that one could obtain a situation which is more single-bandlike. This is expected to reduce the critical Coulomb interaction strength for the Mott transition.

Studying the two-site version of the model, which also includes second-order processes in the nearest-neighbor hopping, we made contact with an effective Kugel-Khomskii Hamiltonian, indicating predominant antiferromagnetic spin fluctuations, an essential ingredient for a prospective superconductor. Antiferromagnetic long-range order is hence also possible and might enhance the tendencies toward an insulating ground state.

[1] See, e.g., A. Ohtomo and H. Y. Hwang, Nature (London) **427**, 423 (2004); N. Reyren, S. Thiel, A. D. Caviglia, L. Fitting Kourkoutis, G. Hammerl, C. Richter, C. W. Schneider, T. Kopp, A.-S. Rüetschi, D. Jaccard, M. Gabay, D. A. Muller, J.-M. Triscone, and J. Mannhart, Science **317**, 1196 (2007).

[2] E. Dagotto, Rev. Mod. Phys. **66**, 763 (1994).

[3] E. Pavarini, I. Dasgupta, T. Saha-Dasgupta, O. Jepsen, and O. K. Andersen, Phys. Rev. Lett. **87**, 047003 (2001).

[4] J. Chaloupka and G. Khaliullin, Phys. Rev. Lett. **100**, 016404 (2008).

[5] P. Hansmann, X. Yang, A. Toschi, G. Khaliullin, O. K. Andersen, and K. Held, Phys. Rev. Lett. **103**, 016401 (2009).

[6] X. Yang, P. Hansmann, A. Toschi, K. Held, G. Khalliulin, and O. K. Andersen (unpublished); see also APS March Meeting (unpublished).

[7] S. S. A. Seo, M. J. Han, G. W. J. Hassink, W. S. Choi, S. J. Moon, J. S. Kim, T. Susaki, Y. S. Lee, J. Yu, C. Bernhard, H. Y. Hwang, G. Rijnders, D. H. A. Blank, B. Keimer, and T. W. Noh, Phys. Rev. Lett. **104**, 036401 (2010).

[8] J. Son, P. Moetakef, J. M. LeBeau, D. Ouellette, L. Balents, S. J. Allen, and S. Stemmer, Appl. Phys. Lett. **96**, 062114 (2010).

[9] N. Chaban, M. Weber, S. Pignard, and J. Kreisel, Appl. Phys. Lett. **97**, 031915 (2010).

[10] R. Arita and K. Held, Phys. Rev. B **72**, 201102(R) (2005).

[11] G. Moeller, Q. Si, G. Kotliar, M. Rozenberg, and D. S. Fisher, Phys. Rev. Lett. **74**, 2082 (1995).

[12] R. Bulla, Phys. Rev. Lett. **83**, 136 (1999).

[13] M. Rozenberg, R. Chitra, and G. Kotliar, Phys. Rev. Lett. **83**, 3498 (1999).

[14] A. Koga, N. Kawakami, T. M. Rice, and M. Sigrist, Phys. Rev. B **72**, 045128 (2005).

[15] M. Ferrero, F. Becca, M. Fabrizio, and M. Capone, Phys. Rev. B **72**, 205126 (2005).

[16] L. de'Medici, A. Georges, and S. Biermann, Phys. Rev. B **72**, 205124 (2005).

[17] A. I. Poteryaev, M. Ferrero, A. Georges, and O. Parcollet, Phys. Rev. B **78**, 045115 (2008).

[18] V. I. Anisimov, I. A. Nekrasov, D. E. Kondakov, T. M. Rice, and M. Sigrist, Eur. Phys. J. B **25**, 191 (2002).

[19] E. Jakobi, N. Blümer, and P. van Dongen, Phys. Rev. B **80**, 115109 (2009).

[20] L. de'Medici, S. R. Hassan, M. Capone, and X. Dai, Phys. Rev. Lett. **102**, 126401 (2009).

[21] Note, in the case of the $LaAlO_3/LaNiO_4$ heterostructures, the $3z^2-r^2$ orbital points toward the insulating AlO layers. Since these are insulating the hopping in z direction is strongly reduced and can approximately be neglected.

[22] J. E. Hirsch and R. M. Fye, Phys. Rev. Lett. **56**, 2521 (1986).

[23] K. Held and D. Vollhardt, Eur. Phys. J. B **5**, 473 (1998).

[24] A. Toschi, A. A. Katanin, and K. Held, Phys. Rev. B **75**, 045118 (2007).

[25] A. A. Katanin, A. Toschi, and K. Held, Phys. Rev. B **80**, 075104 (2009).

[26] C. Huscroft, M. Jarrell, Th. Maier, S. Moukouri, and A. N. Tahvildarzadeh, Phys. Rev. Lett. **86**, 139 (2001).

[27] G. Keller, K. Held, V. Eyert, D. Vollhardt, and V. I. Anisimov, Phys. Rev. B **70**, 205116 (2004).

[28] A. I. Poteryaev, J. M. Tomczak, S. Biermann, A. Georges, A. I. Lichtenstein, A. N. Rubtsov, T. Saha-Dasgupta, and O. K. Andersen, Phys. Rev. B **76**, 085127 (2007).

[29] However, since there is no symmetry breaking involved in the transition, the double occupation is no *real* order parameter.

[30] J. C. Slater and G. F. Koster, Phys. Rev. **94**, 1498 (1954).

[31] O. K. Andersen, W. Klose, and H. Nohl, Phys. Rev. B **17**, 1209 (1978).

[32] E. Koch, O. Gunnarsson, and R. M. Martin, Phys. Rev. B **60**, 15714 (1999).

[33] E. Pavarini, A. Yamasaki, J. Nuss, and O. K. Andersen, New J. Phys. **7**, 188 (2005).

[34] A. Yamasaki, M. Feldbacher, Y.-F. Yang, O. K. Andersen, and K. Held, Phys. Rev. Lett. **96**, 166401 (2006).